Nonionic Surfactant Reverse Micelles of $C_{12}E_4$ in Dodecane: Temperature Dependence of Size and Shape

A. Merdas,[⊥] M. Gindre,[§] R. Ober,[‡] C. Nicot,[§] W. Urbach,*[,†] and M. Waks[§]

Laboratoire de Physique Statistique, URA 1302 CNRS, Ecole Normale Supérieure, 24 rue Lhomond, 75005 Paris, France, Laboratoire de la Matière Condensée, URA 792 CNRS, Collège de France, 10 Place Marcelin Berthelot, 75005 Paris, France, Laboratoire d'Imagerie Paramétrique, URA 1458 CNRS, Université Pierre et Marie Curie, 15 rue de l'Ecole de Médecine, 75006 Paris, France, and Laboratoire de Systèmes Moléculaires Organisés, Université René Descartes, 45 rue des Saints Pères, 75006 Paris, France

Received: February 29, 1996; In Final Form: June 11, 1996[⊗]

We have determined the boundaries of the single-phase water-in-oil microemulsion region of a ternary system (tetraethylene glycol monododecyl ether−dodecane−water) in the oil-rich corner of the phase diagram, as a function of water content and temperature. We have investigated the structures of reverse micelles at temperatures between the lamellar (LC) phase transition and the two-phase separation. Characterization studies have been carried out by dynamic quasi-elastic light scattering and small-angle X-ray scattering as well as by viscosity measurements. It was found that a consistent interpretation of the experimental results requires the complementarity of the above techniques. At a constant water-to-surfactant molar ratio of 13.7, the emerging picture of the isotropic phase is that near the two-phase boundary, micelles behave as slightly solvated spheres of 52-Å radius. With decreasing temperature and as the LC transition is approached, prolate aggregates, displaying an asymmetry of 6 ± 2 are formed and can be considered to be a progressive structural change on the way to lamellae. The physical properties of the system reported herein may have implications for the investigation of proteins in membrane-mimetic media.

Introduction

Ionic and nonionic surfactants in hydrocarbon solvents can solubilize large amounts of water by forming thermodynamically stable microaggregates, generally designated as reverse micelles or microemulsions. These assemblies have received much attention in the last decades since they can host enzymes or other biologically important macromolecules within their water core.[1−4] Their environment, constituted by a continuous organic phase, offers an adequate medium for biotransformations, which have found a number of applications.[5−6] Besides possible industrially important processes due to the remarkable solubility properties of these microspheres, they have also been used as membrane-mimetic systems.[7−8] However, the major part of such studies has been devoted to proteins in ionic surfactants. In particular, we have documented the properties of membrane proteins incorporated into sodium bis(2-ethyhexyl) sulfosuccinate (AOT) reverse micelles in isooctane.[9−13] For the study of interactions between proteins and the micellar interface, nonionic surfactants display, in our opinion, interesting properties by avoiding strong electrostatic interactions which are often held responsible for the destabilization of protein structures.[14] Furthermore, the absence of charges on the surfactant headgroups allows us to assess the importance of hydrophobic forces in the bilayer insertion mechanism and the stability of hydrophobic proteins or peptides.[15]

Nonionic surfactants, especially of the *n*-alkyl poly(ethylene glycol) ether (C_iE_j) type, offer to the investigator a number of advantages compared to their ionic counterparts: (i) the high purity of the surfactants; (ii) the wide selection of the length of polar and nonpolar chains available; (iii) the rich phase behavior of the ternary system C_iE_j−oil−water, which allows us to explore various structural phases. Moreover, no cosurfactant is required for solubilization of water in the alkane phase.

Through the phase prism of such a ternary nonionic system, one finds a constant sequence of phases as a function of increasing temperature due to a gradual change of the mean curvature of the surfactant film.[16−19] About the hydrophile−lipophile balance (HLB) temperature, the mean curvature is zero and a lamellar phase is often observed. At lower temperatures, the curvature is toward the oil, leading to oil-in-water (normal) structures. With increasing temperatures, the curvature is toward the water and water-in-oil (reverse) structures are observed. So one can expect a manifestation of symmetry between normal and reverse structures about the HLB temperature.[20] Much attention has been devoted to the aggregate structure evolution at the inversion of the film surfactant curvature and at equal concentrations of water and oil. Bicontinuous microemulsions of variable connectivity have been observed, as well as disconnected droplets, by NMR self-diffusion,[21−24] X-ray scattering,[25] freeze-fracture electron microscopy,[24−26] and small-angle neutron scattering.[19] Thus, in ternary systems, the size, shape, polydispersity, and interactions between the aggregates varies continuously with temperature and concentration.[27]

The primary focus of this paper is to present a comprehensive study of reverse micelles of the surfactant tetraethylene glycol monododecyl ether in dodecane, at low water and surfactant concentrations. Relatively few studies have been performed in the oil-rich corner of the phase diagram. Given our interest in membrane protein solubilization, the surfactant $C_{12}E_4$ has been selected rather than the more documented $C_{12}E_5$ because of its lower HLB temperature, which provides proteins optimal conditions for retaining their native conformation upon incorporation. Its phase diagram at different temperatures made with various solvents has been reported earlier;[20,28−31] for example,

* E-mail: urbach@physique.ens.fr.
† Ecole Normale Supérieure.
‡ Collège de France.
§ Université Pierre et Marie Curie.
⊥ Université René Descartes.
⊗ Abstract published in *Advance ACS Abstracts,* August 15, 1996.

S0022-3654(96)00628-4 CCC: $12.00

with dodecane, the HLB temperature is located around 25 °C.[20] A two-dimensional phase diagram giving the precise limits of the microemulsion phase as a function of both temperature and water-to-surfactant ratio is presented. To obtain further insights concerning the shape and the size of reverse micelles at a microscopic level above HLB temperature, structural determinations have been carried out using viscosity, dynamic quasi-elastic light scattering (DQLS), and small-angle X-ray scattering (SAXS). The data provide a self-consistent picture with a sharp transition at 29.2 °C from a liquid crystal (LC) to the isotropic phase. In the latter, they reveal, near the transition, particles displaying a prolate shape and an hydrodynamic radius which decreases at higher temperatures. Near the two phase boundary (38.5 °C), micelles are described as slightly solvated spherical droplets.

Experimental Section

1. Materials. The nonionic surfactant $C_{12}E_4$ (tetraethylene glycol monododecyl ether) was purchased from Nikko Chemicals and judged to be >99% pure from gas chromatography. Anhydrous dodecane > 99% pure was from Aldrich and kept under argon. Water used in this study was obtained from a MilliQ system.

2. Determination of Phase Boundaries and Critical Micellar Concentration (cmc) Values. Phase boundaries of the microemulsion region were determined in a closed glass vessel immersed in a thermostated water bath, as described by Aveyard et al.[32] Water was added with a Hamilton microsyringe to mixtures of different surfactant concentrations in dodecane under magnetic stirring, until the onset of permanent turbidity. As specified by Eicke,[33] the bluish appearance of the system was not considered to indicate the beginning of turbidity. The maximum amount of water solubilized in dodecane solutions of $C_{12}E_4$ was then plotted against surfactant concentration at several temperatures. The intercept of the linear water uptake curve with the abcissa yields the minimum surfactant concentration required for the onset of the formation of microemulsion droplets and is defined as the cmc.[32,34] The slope of the curve yields the composition of the droplets at the phase boundary, expressed as the molar ratio of water to surfactant:

$$W_{0_{mic}} = [H_2O]/([C_{12}E_4] - [C_{12}E_4]cmc) \qquad (1)$$

More precise values of the cmc (required for the proper dilution of samples) were determined using a thermostated spectrophotometer to detect the turbidity. The spectrophotometer, a Cary Model 118, was set at a wavelength of 450 nm and the absorption variation recorded. For a given temperature, the experiment was stopped when a permanent increase of 0.02 in optical density was observed. Measured values of the cmc at 30, 35, 40, and 45 °C were respectively 1.0 ± 0.2, 1.7 ± 0.2, 2.4 ± 0.15, and 3.2 ± 0.1 g/per 100 mL.

3. Sample Preparation. The samples were prepared by weighing on a Model 1712 Sartorius balance, directly into a glass ampule, all three components of the system and subsequently carefully mixing. During the experimental procedures, all the samples were prepared at a $W_{0_{mic}}$ value of 13.7 and maintained at a constant water-to-surfactant ratio of the droplets. Since in reverse micelles the cmc at which micelles begin to form is higher than 10^{-3} M, dilution had to be carried out with the continuous phase solvent containing the surfactant at the cmc, so as to maintain the solution equilibrium without removing the surfactant from the micelles.

4. Density Measurements. They were carried out on a Paar DMA 45 or 58 Digital densimeter thermostated at the desired temperature. The partial specific volume (V_D) of the droplets has been determined according to[35]

$$V_D = 1/\rho_S[1 - (\rho_D - \rho_S)/C] \qquad (2)$$

where ρ_S and ρ_D are the densities of the solvent and of the droplet solution, respectively, and C is the droplet concentration in g/mL (water + $C_{12}E_4$). The value of $V_D = 1.02 \pm 0.3$ mL/g was found for droplets at $W_{0_{mic}}$ of 13.7. Calculations of V_D assuming the additivity of the volumes of surfactant and water after mixing with dodecane led to the same value: accordingly, all the samples were prepared directly by weight. Determination of the partial specific volume of the $C_{12}E_4$ surfactant in dodecane led to a molecular volume of 647 Å^3.

5. Small-Angle X-ray Scattering (SAXS). Samples were filled at 30 °C in Lindeman capillaries of 1-mm diameter and sealed. The X-ray generator was a copper rotating anode machine operating at 40 kV and 25 mA. The X-ray apparent source had dimensions 0.1 mm × 0.1 mm. A vertical mirror acted as a total reflector for the $\lambda_{K\alpha} = 1.54$ Å wavelength, eliminated shorter wavelengths of the beam, and directed the X-rays on the positive proportional counter. A nickel filter attenuated the Kβ waves. The dimensions of the beam on the counter were 3 mm vertically and 0.3 mm horizontally. The counter had a window of 3-mm height, a 50-mm useful length, and a 200-μm spatial resolution. The distance between the sample and the counter was 802 mm.[36]

The SAXS data were analyzed using the general equation for the scattered intensity derived by Guinier and Fournet.[37] For polydisperse spherical particles, the log-normal distribution ($N(R)$) is used to represent the particle size distribution

$$N(R) = \frac{dR}{\sigma R\sqrt{2\pi}} \exp\left[-\frac{1}{2\sigma^2}(\ln(R) - \ln(R_0))^2\right] \qquad (3)$$

where $N(R)$ is the number of particles having a radius between R and $R + dR$, the square of the standard deviation (σ) is

$$\sigma^2 \simeq \frac{\langle R^2\rangle - \langle R\rangle^2}{\langle R^2\rangle} = {\sigma_p}^2 \qquad R_0 = \langle R\rangle \exp\left(-\frac{\sigma^2}{2}\right) \qquad (4)$$

and $\langle R\rangle$ is the average radius of the distribution and σ_p the indice of polydispersity. The scattering intensity from spherical particles was expressed by[38]

$$I(q) = \sum_3 N(R)\, R^6\, F_R(q) \qquad (5)$$

$F_R(q)$ is the shape factor ($F_R(0) = 1$) for a sphere with radius R, and $q = (4\pi/\lambda)\sin(\theta/2)$. The analysis was carried out at large q values where the scattering intensity is not too sensitive to particle interaction. Values of $<R>$ and σ were obtained from a curve fitting of $q^4I(q)$ by a least-squares method. For small polydispersity values, the data obtained are not very dependent on the type of distribution. All the dimensions obtained by X-ray scattering are related to the polar part of the particles (i.e., water and the polar headgroup of the surfactant).

From $I(q)$, the pair distribution, $P(r)$, which is the distance histogram of the particle, is obtained by[38]

$$P(r) = \frac{1}{2}\pi^2 \int_0^\infty I(q)\sin(qr)\, dq \qquad (6)$$

6. Dynamic Quasi-Elastic Light Scattering (DQLS). Such measurements allow the determination of the size of aggregates as well as the characterization of their interactions.[39] The experiments were performed using a laboratory-built autocor-

relator. The autocorrelation function was measured in 105 points grouped in 4 zones with different sampling times. This allows a precise determination of both short time and asymptotic behaviour of the autocorrelation function in the same run. The correlator was interfaced to a computer, allowing the continuous control of the baseline. Due to the low scattering power of some samples, occasional dust particles can seriously disturb the results. This problem was solved by introducing a check procedure: at the end of each run, the baseline was calculated and compared to the value measured in the last channel. If the discrepancy was $>5 \times 10^{-3}$ of the signal amplitude, the data were rejected; if the discrepancy was under that value, the data were stored in the computer. At least 100 runs per experiment were collected. The autocorrelation function of scattered intensity was fitted with the following expression:

$$\langle I(t)I(t+\tau)\rangle = 1 + k\mathrm{e}^{-2(t/\tau)} \qquad (7)$$

where $\tau^{-1} = D_c q^2$.[40] D_c is the collective diffusion coefficient, and q, the scattering wave vector, is given by

$$q = \frac{4n\pi}{\lambda}\sin\left(\frac{\theta}{2}\right)$$

where n is the refractive index of the sample and λ is the wavelength of the incident light (5145 Å). The scattering angle (θ) was varied between 30 and 150°.

7. Viscosity. It was measured with Ubberholde and Ostwald capillary viscosimeters in a water bath where the temperature was maintained to ±0.1 °C by a Polystat 1 thermostat. The relative viscosity, $\eta_r = (\eta/\eta_0)$, was measured by comparing the flow time of the microemulsion through the capillary with that of the continuous phase containing the surfactant at the cmc.

Results and Discussion

Microemulsion Single-Phase Stability Regions. In reverse ternary systems composed of a nonionic surfactant, water and oil, the strong temperature dependence of the phase behavior arises in the first place from the variation of the local concentration of water in the ethylene glycol layer, which modulates the surfactant film curvature.[41] But it also originates from the solubility variation of the surfactant monomer in the organic phase occurring as a function of temperature. Taking into account both phenomena,[16] we have determined the extent of the single-phase microemulsion by the procedure described in the Experimental Section.

The maximum solubility of water (in grams per 100 mL of final solution) has been measured at several temperatures, as a function of surfactant concentration in dodecane. We have chosen to show such a plot at 29 °C in Figure 1. Interestingly, at that temperature, successive additions of water lead to water-poor and water-rich isotropic phases. Curve a represents the boundary between the water-poor isootropic phase and a two-phase system. Curve b represents the boundary between the two-phase system and the water-rich isotropic phase. Finally, a two phase system corresponding to water in excess appears as curve c.

At each temperature studied, the plots were linear within experimental error. From the slope of the curves, the droplet composition at different phase boundaries ($W_{0_{mic}}$, eq 1) is obtained, which takes into account the amount of surfactant monomers represented by the intercept with the abcissa. The linearity of the plot suggests that the droplet composition ($W_{0_{mic}}$) is independent of surfactant concentration[32] within the range (2−12% w:v) studied.

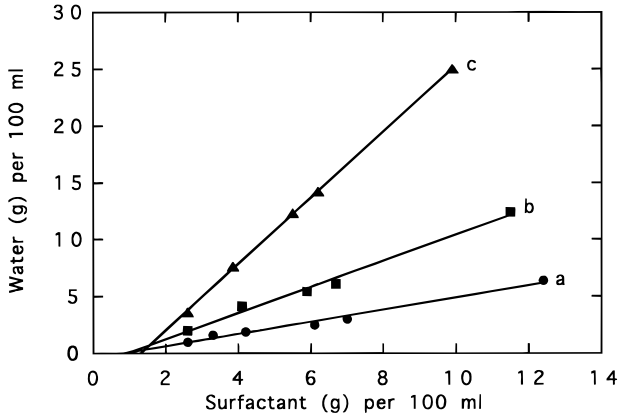

Figure 1. Water uptake curves for solutions of $C_{12}E_4$ in dodecane along several phase boundaries, at 29 °C. Water and surfactant are expressed in grams per 100 mL of final solution. Curve a delineates the boundary of water-poor isotropic phase; curves b and c delineate that of the water-rich isotropic phase. The LC phase is located between curves a and b together with a two-phase system (as shown on Figure 2). Above curve c, separation of water excess occurs.

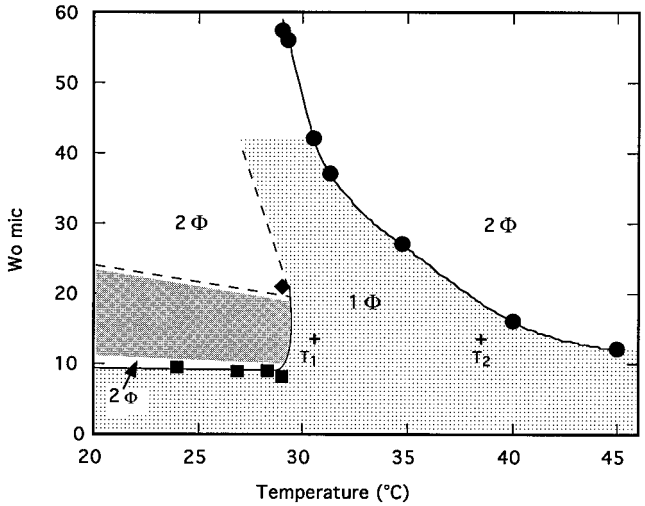

Figure 2. Phase diagram showing the single-phase microemulsion boundaries delineated by the maximum $W_{0_{mic}}$ as a function of temperature. The darkest area represents the LC phase. The dotted area represents the isotropic phase. The dashed line indicates approximative boundaries. T_1 and T_2 are the coordinates of the samples studied in this report.

The variation of $W_{0_{mic}}$ as a function of temperature is illustrated on the phase diagram of Figure 2: it shows the boundaries delimitating the single-phase microemulsion region. Below 29.2 ± 0.3 °C, the boundary delineates a water-poor microemulsion domain ($W_{0_{mic}} < 10$). Due to a bad contrast between solute and solvent, aggregates could not be detected by our DQLS equipment; such micelles have been documented elsewhere.[29,30,42] Furthermore, below 29.2 °C, by increasing the water content, one obtains a two-phase system and then a LC phase, birefringent between crossed polarizers and displaying increased viscosity. The upper limit of the LC phase diagram was not determined in this set of experiments. At 29.2 °C, the boundary displays a "nose-shaped" region,[32] indicating the maximum temperature at which the LC phase can exist. Note that the transition between the LC phase and microemulsion is very sharp (±0.1 °C) without formation of a two phase system. Above 29.2 °C, the surfactant is able to solubilize larger amounts of water (up to $W_{0_{mic}} = 56$), leading to a water-rich isotropic phase. Above an approximate value of $W_{0_{mic}}$ of 20, the micellar solution displays the bluish appearance described by Eicke.[33]

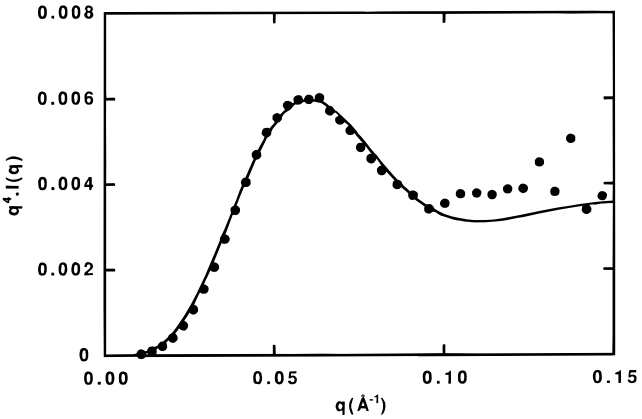

Figure 3. Comparison of experimental data obtained at 38.5 °C, at $\Phi_S = 0.035$ with the theoretical curve $q^4I(q)$ vs q (—) assuming noncorrelated particles. $R_0 = 37.8$ Å; $\sigma = 0.24$.

At higher temperatures and as a function of the water content of the system, the separation of an excess water phase occurs.

Note that such a phase diagram plotted as a function of temperature is usually represented at a single surfactant concentration.[31,43] In contrast, the diagram depicted in Figure 2 is valid for any concentration in the 2−12% w/v surfactant range. It corresponds to the oil-rich corner of the prism diagram. It should also be kept in mind that, as a consequence, the diagram represented in Figure 2 will remain unchanged during all the experiments which require dilutions for the extrapolation of data to zero surfactant concentration.

Micellar Size and Shape. In the temperature range extending from the LC phase to the two-phase separation boundaries, the micelle size and shape as well as their interactions remain a subject of debate and discussion.[16,17] The water-in-oil micelles are less documented than their oil-in-water counterparts located at the water-rich corner under the HLB.[16,18] Experiments were therefore carried out on micelles at a $W_{0_{mic}}$ value of 13.7, at temperatures of 30.5 and 38.5 °C (T_1 and T_2 on Figure 2). Various physical techniques were employed to obtain a more precise picture of the isotropic phase.

SAXS Measurements. In SAXS experiments, the scattering intensity originates from the contrast between electronic densities of the aqueous core which include water and the polar headgroup (poly(ethylene glycol) ether) and that of dodecane comprising the surfactant aliphatic tails. A typical analysis of micellar polydispersity at 38.5 °C and at $W_{0_{mic}}$ of 13.7 is shown in Figure 3. The fit of $q^4I(q)$ vs q was carried out for q values between 0.09 and 0.16 Å^{-1}. The curves were fitted for a sphere distribution with a radius $R_0 = 37.8$ Å and $\sigma = 0.24$ at 38.5 °C (Figure 3) and with a radius $R_0 = 40$ Å and $\sigma = 0.24$ at 30.5 °C. At low q values, the experimental curve $I(q)$ vs q displays deviation from the theoretical curve for polydisperse spheres (Figure 4). At 38.5 °C, the deviation originates from repulsive interactions between spherical droplets. At 30.5 °C, the observed deviation may arise either from attractive interactions or from anistropic aggregates. Indeed, in the latter case, the curve $q^4I(q)$ could be fitted by a cylinder displaying a radius R between 34 and 39 Å. It should be stressed that the radii of both the sphere and the cylinder remain constant at all the values of Φ, the micellar volume fraction, studied in this set of experiments, as verified.

In order to gain further information concerning the shape of the particle, the pair distribution curve, $P(r)$, was computed from the measured $I(q)$. At 38.5 °C, $P(r)$ is characteristic of spheric particles, while at 30.5 °C, $P(r)$ is characteristic of anisotropic noncorrelated particles, with a maximum length in the 350−380-Å range (Figure 5). Nevertheless, since the above results cannot unambiguously establish the structure of the particle, additional experiments have been carried out.

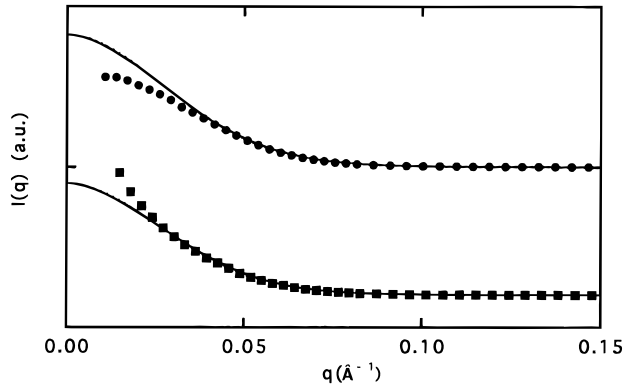

Figure 4. Comparison of experimental data at 30.5 °C (◆) and 38.5 °C (●) with theoretical curves $I(q)$ vs q (—) Note the deviation from the theoretical curve at low q values.

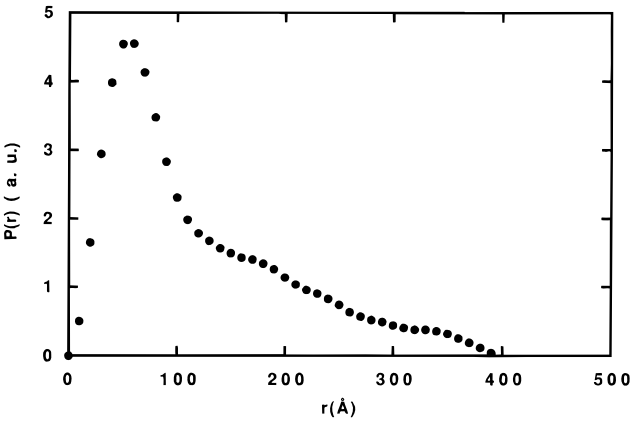

Figure 5. Pair distance distribution function $P(r)$ obtained from $I(q)$ at 30.5 °C and $\Phi = 0.035$, using eq 6.

DQLS Measurements. In the limit of zero micellar volume fraction (Φ), one can write

$$\lim D_c(\Phi) = D_0 = \frac{kT}{6\pi\eta R_h} \tag{8}$$

where k is the Boltzmann constant, T is the absolute temperature, η is the viscosity of the continuous phase, and R_h is the hydrodynamic radius of the particle. For low Φ values,

$$D_c = D_0(1 + \alpha_c\Phi) \tag{9}$$

where α_c is the first virial coefficient and contains contributions of hydrodynamic and direct interactions. The more complete calculations of α_c are those of Felderof[44] and Batchelor,[45] who assume two-body hydrodynamic interactions and found $\alpha_c \sim 1.5$. The results of the DQLS experiments are shown in Figure 6 and summarized in Table 1. At 30.5 °C, a value of 117 ± 3 Å is obtained for R_h; however, when the temperature is increased to 38.5 °C, a much lower value of 53 Å is found. At the same temperature, the value found for α_c is -0.9 ± 0.2. Recently, some attempts to take into account four-body interactions have been reported,[46] leading to a similar value for hard spheres but somewhat different from 1.5.

Viscosity. Additional information about the shape and/or the solvation of the aggregates can be obtained by viscosity measurements. Plots of η_{spe}/c vs c, the droplet weight concentration, are shown at three temperatures in Figure 7. The

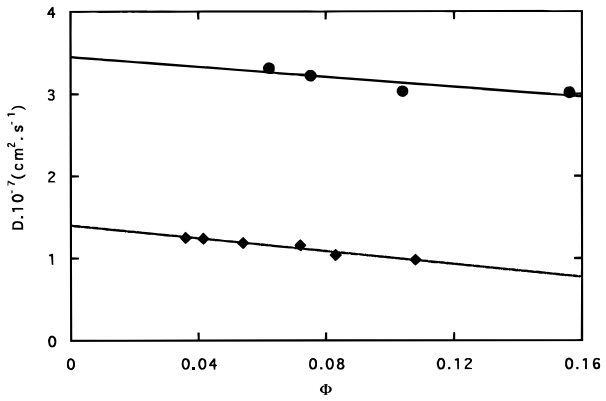

Figure 6. Diffusion coefficients measured as a function of the micelle volume fraction Φ. Collective diffusion coefficient D_c measured by DQLS at temperatures of 30.5 °C (◆) and 38. 5 °C (●).

TABLE 1: Summary of Data Obtained by SAXS[a] and DQLS[b]

T, °C	R,[a] Å	D_c,[b] cm^2 s^{-1}	α_c[b]	R_h,[b] Å
30.5	48 ± 0.2	1.40×10^{-7}	−2.8 ± 0.8	117 ± 3
38.5	45.8 ± 0.2	3.45×10^{-7}	−0.9 ± 02	53 ± 3

[a] Micelle radius assuming a spherical shape, obtained by the addition of the hydrocarbon tail length (8 Å) to the polar core radius measured by SAXS. [b] D_c is the collective diffusion coefficient. α_c is the first virial coefficient of D_c. R_h is the corresponding hydrodynamic radius.

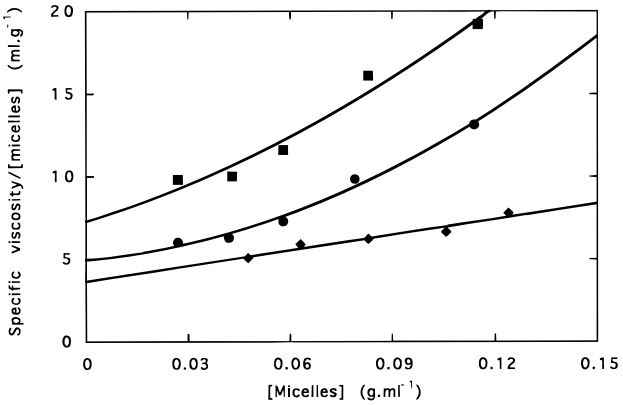

Figure 7. Determination of intrinsic viscosities and Huggins coefficient from viscometry at different temperatures: 30. 5 °C (■), 33 °C (●), 38.5 °C (◆).

data were analyzed according to

$$\frac{\eta_r - 1}{c} = \frac{\eta_{spe}}{c} = [\eta] + K_H[\eta]^2 c + ... \qquad (10)$$

which neglects higher terms in c. The Huggins coefficient, K_H, determined from the initial slope of the curves, reflects the interparticle interactions. For hard spheres, theoretical values of K_H are 0.7[47] or 1.0,[48] both attractive and repulsive potentials leading to an increase of the coefficient.

The intrinsic viscosity, $[\eta]$, is found as the intercept with the y axis. Its value is relatively unaffected by the size of the aggregates and provides information about their shape and/or their solvation as expressed by[49]

$$[\eta] = \nu(V_D + V_s\delta) \qquad (11)$$

where the Einstein−Simha factor, ν, contains all the shape dependence (2.5 for a hard sphere). V_D and V_S are the partial specific volume of the droplet and of the solvent respectively;

TABLE 2: Parameters Derived from Viscosity Data[a]

					sphere		
T, °C	$[\eta]$, cm^3 g^{-1}	K_H	V_s, cm^3 g^{-1}	V_D, cm^3 g^{-1}	δ, g/g	n_{solv}	R_{solv}, Å
30.5	7.3 ± 2.6	1.29 ± 1	1.35	1.02	1.4	5	68
33.0	4.9 + 1.2	0.75 ± 0.5					
38.5	3.6 ± 0.4	0.65 ± 0.2	1.36	1.03	0.3	1	51

[a] V_S: partial-specific volume of the surfactant. V_D: partial-specific volume of the droplet. If a spherical shape is assumed for the micelle, δ is the the weight of the bound solvent in grams per gram of droplet, n_{solv} is the number of solvent molecules per surfactant molecule, and R_{solv} is the calculated radius of the solvated micelle.

δ is the weight of the solvent associated with 1g. of droplets. Values of viscosity measurements are given in Table 2. As the temperature increases, a progressive decrease of the intrinsic viscosity is observed, together with the initial slope of the curve (Figure 7) reflected by the decrease of the Huggins coefficient. Hence, it appears that the droplet shape near the two-phase separation is close to spherical, as described in other similar systems.[16]

Structural Features of the Microemulsion. In order to enable a better understanding of the system, SAXS and viscosity data have been associated. Assuming a hard-sphere potential for the droplets ($\nu = 2.5$), then from eq 11 and from viscosity results, we calculate the maximal solvation degree, δ, expressed in grams of solvent by grams of droplets or by the number of molecules of solvent per surfactant molecule (Table 2). The radius of the spherical unsolvated micelle is obtained from SAXS results (Table 1) by adding to the radii of the aqueous core the C_{12} tail length of 8 Å, in accordance with recent literature.[50] Then we calculate from simple geometrical considerations the radii of the solvated spherical micelles at the two temperatures studied: the radii are 68 and 51 Å at 30.5 and 38.5 °C, respectively (Table 2). At 38.5 °C, the solvation of a spherical particle can account for the value of $R_h = 53$ Å obtained by DQLS, a result consistent with α_c and Huggins coefficient values. The repulsive interactions observed on the $qI(q)$ curve at low q values are also in accordance with a hard-sphere model for the particle.

In contrast, at 30.5 °C, the assumption of a spheric solvated micelle cannot hold (R_h = 117 Å by DQLS). At this temperature, the interpretation of all the data seems in good agreement with the presence of an asymmetric particle. If we assume solvation to be negligible ($\delta = 0$), then eq 11 can be written as $[\eta] = \nu V_D$, allowing for the estimation of the Einstein−Simha factor ($\nu = 7.2$) for maximal assymmetry. From its value, the axial ratio for an ellipsoid can be calculated by the Simha equation.[51] If we define p as the ratio of revolution to equatorial axes of the micelle, then the calculated value of p for an oblate shape of the aggregate is 1/9 ± 0.02, while for a prolate shape, $p = 6 \pm 2$. The value of $p = 4.4 \pm 0.3$ calculated from the dimensions of the cylinder obtained from SAXS measurements is therefore in good agreement, within the error limits of p for the prolate shape.

From these data, an R_h value can be calculated. Let the mean cylinder radius (36.5 + 8 Å = 44.5 Å) as determined by SAXS at 30.5 °C be equal to the small semiaxis of an ellipsoid; then we are able to calculate the ellipsoid volume and the radius of the sphere of equivalent volume R_{equ}. Depending on the shape of the particle, p is related to the function $f(p)$ by Perrin's equations,[52] which is

$$f(p) = p^{1/3}(p^2 - 1)^{-1/2} \ln[p + (p^2 - 1)^{1/2}] \quad \text{with } p > 1 \qquad (12)$$

TABLE 3: Size Parameters[a] Assuming a Prolate or an Oblate Shape for Micelles at 30.5 °C

	p	$(f)p$	R_h, Å
prolate	6 ± 2	0.76	121 ± 22
oblate	$1/9 \pm 0.02$	0.71	322 ± 28

[a] Calculated fromSAXS and viscosity data assuming $\delta = 0$. p is the ratio of revolution to equatorial axes.

for a prolate and

$$f(p) = p^{1/3}(1 - p^2)^{-1/2} \arctan[(1 - p^2)^{1/2}p] \quad \text{with } p < 1 \tag{13}$$

for an oblate.

The function $f(p)$ allows us to calculate the hydrodynamic radius (R_h) from

$$R_h = \frac{R_{equ}}{f(p)} \tag{14}$$

Table 3 summarizes the values of p, $f(p)$, and R_h for prolate and oblate shapes of the particle. Assuming a prolate shape, the calculated value of R_h is consistent with the hydrodynamic radii measured by QELS, thus ruling out an oblate shape for the particle. Moreover, the increase of the Huggins coefficient and the slight decrease of α_c imply attractive interactions between the prolate micelles.

In ternary mixtures of $C_{12}E_5$−decane−water, successive shape transitions from sphere to cylinder and then to lamellae have been also documented in normal (as opposed to reverse) micelles as a function of increasing temperature.[18] This is yet another example of the symmetry taking place around the HLB temperature between normal and reverse amphiphilic structures.[20] In this respect, it should also be noted that in a different system ($C_{12}E_5$−heptane−water), the dissymmetry of particles observed by increasing or decreasing the temperature in normal or reverse micelles, was attributed to the interparticle interactions by Clark et al.,[53] using time-resolved fluorescence spectrophotometry. However, from a further paper by the same authors,[32] it appears that our experiments have been carried out in a close but different region of the phase diagram.

Concluding Remarks

As pointed out by Herrington and Sahi,[54] one of the fundamental issues in binary or ternary systems of C_iE_j nonionic surfactants is whether "the effect of temperature is to cause predominantly micelle growth or to increase the strength of the interactions between small micelles". In a system in which many different structural types can be obtained by changing a single parameter, temperature, we believe that we have brought pertinent answers to this question within the limits of the present work. We show indeed that to reach a firm conclusion about these issues requires the combination of several techniques and a careful analysis of data. Taken together, they allow us to discriminate between the possible structures existing in a rather narrow temperature range which can be precisely controlled.

In summary, near the two phase separation boundary, viscosity, SAXS, and DQLS data are consistent with slightly solvated (one dodecane molecule per surfactant) spherical droplets with a 52-Å radius. With decreasing temperatures, on approaching the LC transition, the intrinsic viscosity increases and a much larger R_h value is obtained in the 115−120-Å range by DQLS measurements. SAXS measurements support the proposal that the most consistent shape for the micelles corresponds to a prolate ellipsoid with an asymmetry of 6 ± 2 which can be considered to be the first step on the progressive transition to lamallae.

In the more biological area of membrane-mimetic media, the property of the surfactant phase diagram, by which one transits from a lamellar phase to an optically transparent microemulsion at accessible temperatures, provides an opportunity to follow the self-organizing structures upon incorporation of transmembrane proteins (manuscript submitted).

Acknowledgment. We are grateful to Dr. J. Y. Le Huerou for invaluable editorial help. This work was supported in part by l'Action Concertée "Interface Chimie, Physique, Biologie" du Ministère de l'Enseignement Supérieur et de la Recherche.

References and Notes

(1) Luisi, P. L.; Magid, L. J. *Crit. Rev. Biochem.* **1986**, *20*, 409.
(2) Martinek, K.; Levashov, A. V.; Klyachko, N.; Khmel'nitski, Y. L.; Berezin, I. V. *Eur. J. Biochem.* **1986**, *155*, 453.
(3) Waks, M. *Proteins, Struct. Funct. Genet.* **1986**, *1*, 4.
(4) Verhaert, M. R. D.; Hilhorst, R.; Visser, A. J. W. G.; Veeger, C. *Biomolecules in organic solvents*; CRC: Boca Raton, FL, 1992; Chapter 6.
(5) Oldfield, C. *Biotechnol. Genet. Engin. Rev.* **1994**, *12*, 255.
(6) Komives, C. F.; Lilley, E.; Russell, A. J. *Biotechnol. Bioeng.* **1994**, *43*, 946.
(7) Fendler, J. *Membrane Mimetic Chemistry*; Wiley: New York, 1982; Chapter 10.
(8) . O'Connor, C. J.; Lomax, T D.; Ramage, R. E. *Adv. Colloid Interface Sci.* **1984**, *20*, 21.
(9) Nicot, C.; Vacher, M.; Vincent, M.; Waks, M. *Biochemistry* **1985**, *24*, 7024.
(10) Chatenay, D.; Urbach, W.; Cazabat, A. M.; Vacher, M.; Waks, M. *Biophys. J.* **1985**, *48*, 893.
(11) Chatenay, D.; Urbach, W.; Nicot, C.; Vacher, M.; Waks, M. *J. Phys. Chem.* **1987**, *91*, 2198.
(12) Gallay, J.; Vincent, M.; Nicot, C.; Waks, M. *Biochemistry* **1987**, *26*, 5738.
(13) Binks, B. P.; Chatenay, C.; Urbach, W.; Waks, M. *Biophys. J.* **1989**, *55*, 949.
(14) Honig, B.; Nicholls, A. *Science* **1995**, *268*, 1144.
(15) Jones, D. J.; Gierasch, L. M. *Biophys. J.* **1994**, *67*, 1546.
(16) Aveyard, R.; Binks, B. P.; Fletcher, P. D. I. *Langmuir* **1989**, *5*, 1210.
(17) Olsson, U.; Wurz, U.; Strey, R. *J. Phys. Chem.* **1993**, *97*, 4535.
(18) Leaver, M. S.; Olsson, U.; Wennerstrom, H.; Strey, R. *J. Phys. II Fr.* **1994**, *4*, 515.
(19) Lee, D. D.; Chen, H. *Phys. Rev. Lett.* **1994**, *73*, 106.
(20) Kunieda, H.; Nakamura, K.; Davis, H. T.; Evans, D. F. *Langmuir* **1991**, *7*, 1915.
(21) Olsson, U.; Shinoda, K.; Lindman, B. *J. Phys. Chem.* **1986**, *90*, 4083.
(22) Olsson, U.; Nagai, K.; Wennerstrom, H. *J. Phys. Chem.* **1988**, *92*, 6675.
(23) Anderson, D. M.; Wennerstrom, H. *J. Phys. Chem.* **1990**, 94, 8683.
(24) Bodet, J. F.; Bellare, J. R.; Davis, H. T.; Scriven, L. E.; Miller, W. G. *J. Phys. Chem.* **1988**, *92*, 1898.
(25) Lichterfeld, F.; Schmeling, T.; Strey, R. *J. Phys. Chem.* **1986**, *90*, 5762.
(26) Jahn, W.; Strey, R. *J. Phys. Chem.* **1988**, *92*, 2294.
(27) Barnes, I. S.; Hyde, S. T.; Ninham, B. W.; Derian, P. J.; Drifford, M.; Zemb, T. N. *J. Phys. Chem.* **1988**, *92*, 2286.
(28) Friberg, S.; Lapszynska, I. *Prog. Colloid. Polym. Sci.* **1975**, *56*, 16.
(29) Ravey, J. C.; Buzier, M.; Picot, C. *J. Colloid. Interface Sci.* **1984**, *97*, 9.
(30) Ravey, J. C.; Buzier, M. *ACS Symp. Ser. 272* **1985**, Chapter 16.
(31) Solans, C.; Pons, R.; Zhu, S.; Davis, H. T.; Evans, D. F.; Nakamura, K.; Kunieda, H. *Langmuir* **1993**, 9, 1479.
(32) Aveyard, R.; Binks, B. P.; Fletcher, P. D. I.; Ye, X. *J. Chem. Biotechnol.* **1992**, *54*, 231.
(33) Eicke, H.-F. *J. Colloid Interface Sci.* **1979**, *68*, 440.
(34) Komives, C. F.; Osborne, D. E.; Russel, A. J. *J. Phys. Chem.* **1994**, *98*, 369.
(35) Kaminsky, S. M.; Richards, F. M. *Protein Sci.* **1992**, *1*, 22.
(36) Giasson, S.; Espinat, D.; Palermo, T.; Ober, R.; Pessah, M.; Morizur, M. F. *J. Colloid. Interface Sci.* **1992**, *153*, 355.
(37) Guinier, A.; Fournet, G. *Small Angle Scatter. X-Rays* **1955**, Chapter 6.
(38) Glatter, O. *J. Appl. Crystallogr.* **1979**, *12*, 166.

(39) Chatenay, D.; Urbach, W.; Messager, R.; Langevin, D. *J. Chem. Phys.* **1987**, *86*, 2343.
(40) Koppel, D. E. *J. Chem. Phys.* **1972**, *57*, 4814.
(41) Nilsson, P.-G.; Wennersrtöm, H.; Lindman, B. *J. Phys. Chem.* **1983**, *87*, 1377.
(42) Vasilescu, M.; Caragheorgheopol, A. *Langmuir* **1995**, *11*, 2893.
(43) Kahlweit, M.; Strey, M.; Haase, D.; Kunieda, H.; Schmeling, T.; Faulhaber, B.; Borkovec, M.; Eicke, H.-F.; Busse, G.; Eggers, F.; Funck, T. H.; Richmann, H.; Magid, L.; Söderman, O.; Stilbs, P.; Winkler, J.; Dittrich, A.; Jahn, W. *J. Colloid Interface Sci.* **1987**, *118*, 436.
(44) Felderof, B. U. *J. Phys.* A **1978**, *11*, 927.
(45) Batchelor, G. K. *J. Fluid. Mech.* **1976**, *74*, 1.
(46) Carter, J. M.; Phillies, G. DJ. *J. Phys. Chem.* **1985**, *89*, 5118.
(47) Paterson, M. J.; Fixman, M. J. *J. Chem. Phys.* **1963**, *39*, 2516.
(48) Russel, W. B. *J. Chem Soc., Faraday Trans.* 2 **1984**, *80*, 31.
(49) Scheraga, H. A.; Mandelkern, L. *J. Am. Chem. Soc.* **1953**, *75*, 179.
(50) Klose, G.; Eisenblatter, St.; Galle, J.; Islamov, A.; Dietrich, U. *Langmuir* **1995**, *11*, 2889.
(51) Tanford, C. *Physical Chemistry of Macromolecules;* Wiley: New York, 1961; Chapter 6.
(52) Perrin, J. *J. Phys. Rad.* **1936**, *7*, 1.
(53) Clark, S.; Fletcher, P. D. I.; Ye, X. *Langmuir* **1990**, *6*, 1301.
(54) Herrington, T. M.; Sahi, S. S. *J. Colloid Interface Sci.* **1988**, *121*, 107.

JP960628P